ResearchGate

See discussions, stats, and author profiles for this publication at: https://www.researchgate.net/publication/231655024

Reversibility and Improved Hydrogen Release of Magnesium Borohydride

ARTICLE *in* THE JOURNAL OF PHYSICAL CHEMISTRY C · FEBRUARY 2010

Impact Factor: 4.77 · DOI: 10.1021/jp9116744

CITATIONS
74

READS
19

5 AUTHORS, INCLUDING:

Vitalie Stavila
Sandia National Laboratories
123 PUBLICATIONS **1,655** CITATIONS
SEE PROFILE

Leonard E. Klebanoff
Sandia National Laboratories
79 PUBLICATIONS **1,101** CITATIONS
SEE PROFILE

Available from: Vitalie Stavila
Retrieved on: 02 February 2016

Reversibility and Improved Hydrogen Release of Magnesium Borohydride

Rebecca J. Newhouse,[†,‡] Vitalie Stavila,[*,‡] Son-Jong Hwang,[§] Leonard E. Klebanoff,[‡] and Jin Z. Zhang[†]

Department of Chemistry and Biochemistry, University of California, Santa Cruz, California 95064, Sandia National Laboratories, Livermore, California 94551, and Division of Chemistry and Chemical Engineering, California Institute of Technology, Pasadena, California 91125

Received: December 9, 2009; Revised Manuscript Received: February 4, 2010

Desorption and subsequent rehydrogenation of $Mg(BH_4)_2$ with and without 5 mol % TiF_3 and $ScCl_3$ have been investigated. Temperature programmed desorption (TPD) experiments revealed a significant increase in the rate of desorption as well as the weight percentage of hydrogen released with additives upon heating to 300 °C. Stable $Mg(B_xH_y)_n$ intermediates were formed at 300 °C, whereas MgB_2 was the major product when heated to 600 °C. These samples were then rehydrogenated and subsequently characterized with powder X-ray diffraction (pXRD), Raman, and NMR spectroscopy. We confirmed significant conversion of MgB_2 to fully hydrogenated $Mg(BH_4)_2$ for the sample with and without additives. TPD and NMR studies revealed that the additives have a significant effect on the reaction pathway during both dehydrogenation and rehydrogenation reactions. This work suggests that the use of additives may provide a valid pathway for improving intrinsic hydrogen storage properties of magnesium borohydride.

Introduction

Complex metal hydrides have long been discussed as possible hydrogen storage materials because of their exceptional volumetric and gravimetric densities, yet their high thermal stabilities ostensibly excluded them from consideration as practical, onboard hydrogen storage materials.[1–4] However, after the initial demonstration[5] of low temperature hydrogen release at ~100 °C as well as reversibility with catalyzed $NaAlH_4$, hydrogen release and decomposition pathways of complex metal hydrides have become an active area of research.[6–16]

In particular, magnesium borohydride, $Mg(BH_4)_2$, is a lightweight borohydride that stores 14.9% hydrogen by weight. Early studies of the synthesis and thermal decomposition of $Mg(BH_4)_2$ proved inconsistent, perhaps as a result of premature decomposition from high desolvation temperatures and/or incomplete desolvation.[17–21] It was not until recently that the crystal structures of both the low and high temperature phases (α and β, respectively) were solved.[22–24] Previous studies estimated $\Delta H \approx 40$ kJ/mol H_2, which implies desorption temperatures within the desired range as well as potential reversibility.[25–27] Li et al., however, experimentally determined a higher enthalpy, $\Delta H = 57$ kJ/mol H_2, for the first desorption step.[28] Recent studies revealed a more complicated multistep decomposition pathway than previously thought, with the proposed formation of an amorphous intermediate similar in structure to $MgB_{12}H_{12}$.[29–31] In addition, studies have shown an inverse correlation between electronegativity of the cation and borohydride stability. The Pauling electronegativity of Mg ($\chi = 1.31$) is less than that for Na, Li, and Ca ($\chi = 0.93$, 0.98, and 1.00, respectively), and pure $Mg(BH_4)_2$ has been observed to initiate decomposition around 270 °C, much lower than Li, Na, and Ca borohydride.[32,33] In contrast, titanium borohydride (χ of Ti = 1.54) is unstable at room temperatures.[33,34] Another advantage of $Mg(BH_4)_2$ is that the fully dehydrogenated product is a single phase material, MgB_2[22,29,30]

$$Mg(BH_4)_2 \rightarrow MgB_2 + 4H_2 \quad \text{(I)}$$

In contrast, several other borohydrides of interest, such as $LiBH_4$, $NaBH_4$, and $Ca(BH_4)_2$, decompose to their corresponding binary hydrides. The stabilities of lithium, sodium, and calcium hydrides are formidable and in fact they melt before decomposition at temperatures significantly greater than 600 °C, essentially sequestering the hydrogen. Even above these high temperatures needed for hydride decomposition, there still exists a two phase system of elemental metal and boron species that does not necessarily favor formation of a single phase. This is important since phase separation necessarily hinders reversibility.

Despite the significant advantages of $Mg(BH_4)_2$ over other lightweight borohydrides, further destabilization is desired. Various methods have been successfully applied to complex metal hydrides to promote hydrogen desorption at lower temperatures and reversibility including confinement in nanoporous scaffolds,[35] destabilization with metal hydrides,[11,16] metal oxides[6] and transition metals additives.[5,36,37] Ti-doped $NaAlH_4$ reported by Bogdanović[5,38,39] and the MgH_2-LiBH_4 system presented by Vajo et al.[16] demonstrate the dramatic role additives can have in destabilizing materials to enable much lower temperatures of hydrogen release as well as imparting previously unattainable reversibility. In particular, stoichiometric amounts of $ScCl_3$ and TiF_3 have previously been shown to promote hydrogen release at lower temperatures in borohydrides. $ScCl_3$ milled with $LiBH_4$ results in $LiSc(BH_4)_4$ which starts releasing hydrogen at ~177 °C as opposed to >400 °C for pure $LiBH_4$[32,40] and TiF_3 addition results in hydrogen desorption at <100 °C in $Li(BH_4)_2$.[41] Destabilization of $Mg(BH_4)_2$ has not yet been extensively explored, although recently it has been incorporated into activated carbon, and hydrogen release was observed

* To whom correspondence should be addressed. E-mail: vnstavi@sandia.gov. Phone: 925-294-3059.
† University of California, Santa Cruz.
‡ Sandia National Laboratories.
§ California Institute of Technology.

10.1021/jp9116744 © 2010 American Chemical Society
Published on Web 02/25/2010

starting at 150 °C in comparison to 269 °C for the bulk material.[42] Moreover, $TiCl_3$ milled with $Mg(BH_4)_2$ in the weight ratio of 1:3 was found to reduce the desorption temperature substantially (<100 °C).[43] Reversibility of these systems, however, has not been examined.

Reversibility of pure $Mg(BH_4)_2$ has recently been investigated by several groups. Evidence was reported for ~6 wt % reversible hydrogen storage capability at moderate temperatures and pressure through the proposed intermediate, $MgB_{12}H_{12}$.[31] However, a recent study by Severa et al. showed for the first time full reversibility of $Mg(BH_4)_2$.[44] The authors rehydrogenated commercially available MgB_2 under 95 MPa H_2 and 400 °C to generate $Mg(BH_4)_2$ (reverse reaction **I**), which showed that a complete hydrogenation and dehydrogenation cycle is possible for $Mg(BH_4)_2$.[44]

Demonstrating cyclability and improved desorption are crucial in establishing $Mg(BH_4)_2$ as a practical solution for on-board hydrogen storage. In this study, we used small amounts of TiF_3 and $ScCl_3$ as additives to facilitate hydrogen release and potentially improve reversibility to the completely hydrogenated starting material, $Mg(BH_4)_2$. Temperature programmed desorption (TPD) experiments at 300 °C revealed a significant increase in the rate of desorption and the weight percent of hydrogen released with the additives. PXRD as well as NMR and Raman spectroscopy were employed to further characterize the role of the intermediates and additives during hydrogen release to MgB_2 and rehydrogenation back to the borohydride. The results indicate that using metal halides as additives is a promising direction for improving the sorption kinetics of $Mg(BH_4)_2$ by lowering the energy barriers involved in key reaction processes.

Experimental Procedure

Synthesis and Preparation of $Mg(BH_4)_2$. Magnesium borohydride was synthesized using a variation of a previously published literature procedure.[45] First, 100 mmol of 1 M $Mg(C_4H_9)_2$ in heptane (Sigma Aldrich) was added dropwise by cannula to 400 mmol of $BH_3 \cdot S(CH_3)_2$ (76% in dimethyl sulfide, Sigma Aldrich) in 200 mL of dry toluene, and a white precipitate was formed. The solution was allowed to stir under flowing argon overnight. Excess toluene was removed, then the white precipitate $Mg(BH_4)_2 \cdot 2S(CH_3)_2$ was washed several times with dry toluene and subsequently dried under vacuum at 160 °C overnight to remove complexed $S(CH_3)_2$. The synthesized $Mg(BH_4)_2$ was characterized by powder X-ray diffraction (pXRD) and found to correspond to the low-temperature α phase.[22–24] The $Mg(BH_4)_2$ pattern is distinct from that of the $Mg(BH_4)_2 \cdot 2S(CH_3)_2$ adduct that initially precipitates during the wet chemical synthesis (Figure 1).

The adduct-free $Mg(BH_4)_2$ was ball milled in a SPEX 8000 high-energy mill with both 5 mol % TiF_3 (Aldrich) and 5 mol % $ScCl_3$ (Alfa Aesar, 99.9%) and, for comparison, without additives in a 25 mL tungsten carbide grinding vial with two tungsten carbide balls for a total milling time of 30 min, with 5 min breaks after each 10 min interval.

Characterization. TPD measurements were performed with a PCT-Pro Sievert's apparatus. The hydrogen was initially desorbed into an evacuated calibrated volume. The pressure was monitored with calibrated pressure transducers while the sample was heated to and maintained at 300 and 600 °C, respectively. Rehydrogenation experiments were performed by first pressing thin pellets of the fully desorbed powders and subsequent exposure to 90 MPa of H_2 at 390 °C for 72 h.

Solid-state magic angle spinning NMR (MAS NMR) spectra of various nuclei were measured using a Bruker Avance 500 MHz spectrometer with a 11.7 T magnet and employing a boron-free Bruker 4 mm CPMAS probe. The spectral frequencies were 500.23, 470.7, 160.50, and 121.6 MHz for the ^1H ^{19}F, ^{11}B, and ^{45}Sc nuclei, respectively. Single pulse (0.5 μs-π/12) ^{11}B NMR experiments under MAS condition, with a typical spinning rate of 15 kHz, were performed with strong ^1H decoupling, and ^{11}B cross-polarization (CP) MAS spectra were also obtained occasionally as needed. $^{11}B\{^1H\}$ CP MAS NMR experimental conditions were described in previous publications.[30,46] NMR shifts are reported in parts per million (ppm) when externally referenced to tetramethylsilane (TMS) for ^1H, $BF_3 \cdot Et_2O$ for ^{11}B, $CFCl_3$ for ^{19}F, and an aqueous solution of $Sc(NO_3)_3$ for ^{45}Sc NMR. The powder samples collected after decomposition/absorption reactions were packed into a 4 mm ZrO_2 rotor and sealed with airtight Kel-F cap inside an Ar-filled glovebox. Sample spinning was performed under dry nitrogen gas.

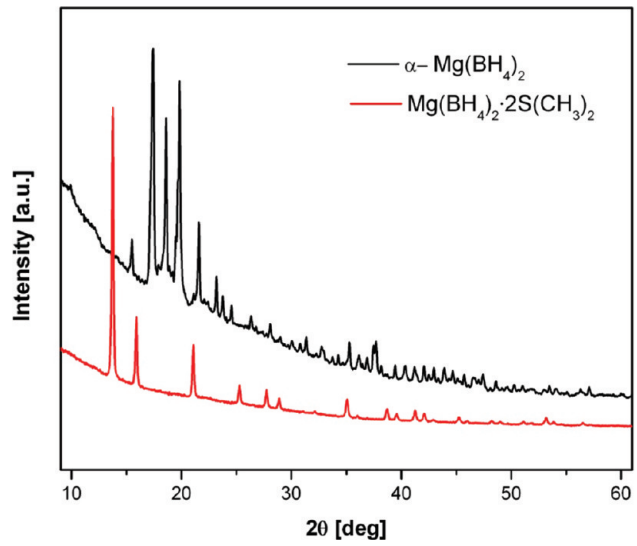

Figure 1. pXRD pattern for the $Mg(BH_4)_2 \cdot 2S(CH_3)_2$ adduct (red line) is distinct from the fully desolvated product, α-$Mg(BH_4)_2$ (black line).

Crystal phase identification pXRD data was collected on a model RU-300 rotating anode Rigaku diffractometer with a Cu-target at 40 kV and 60 mA at 295 K. The powder was contained in a vacuum-grease sealed capillary of 0.7 mm diameter prepared in a glovebox. Raman measurements were obtained using a diode-pumped 532 nm laser directed into an Acton Spectropro-275 monochromator/spectrograph with a 600 g/mm grating. A Princeton Instrument's liquid nitrogen cooled Spec-10 CCD was used to detect the scattered light. The laser power was 0.5 mW on the sample using a 50x objective. SEM images and EDS analysis were obtained using a JEOL JSM-6700F field emission scanning electron microscope.

Results and Discussion

Desolvation of $Mg(BH_4)_2 \cdot 2S(CH_3)_2$ upon heating in vacuum produces pure α-$Mg(BH_4)_2$.[45] The pXRD pattern of the product shown in Figure 1 confirmed that $Mg(BH_4)_2$ was completely desolvated. The sorption kinetic profiles of $Mg(BH_4)_2$ with and without (±) additives were measured and the representative results are presented in Figure 2. Addition of 5 mol % TiF_3 and $ScCl_3$ resulted in a significant increase in both the rate of hydrogen desorption and the ultimate weight percent of hydrogen released. After 17 h at 300 °C, the $Mg(BH_4)_2$ with additives released 9.7 wt % of hydrogen compared to 7.7% for the sample without additives. The weight percent of hydrogen released for

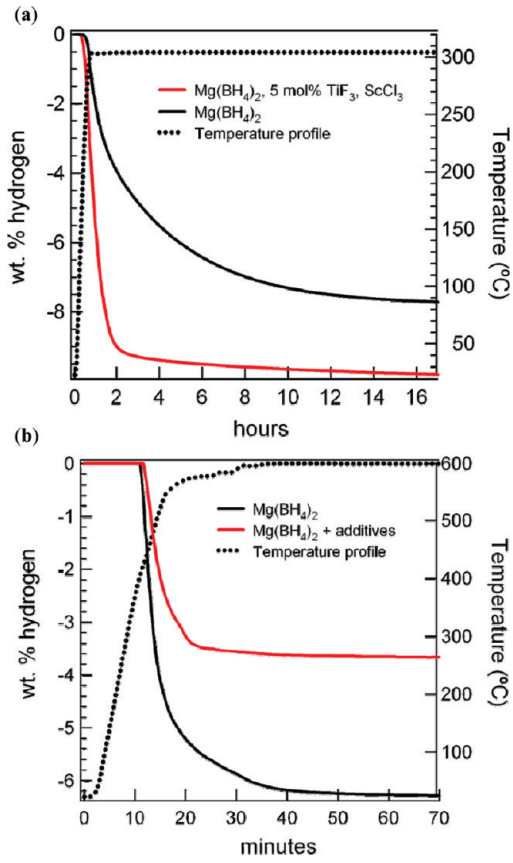

Figure 2. Temperature programmed desorption (TPD) data for $Mg(BH_4)_2$ with 5 mol % TiF_3 and $ScCl_3$ (red line) and the pure $Mg(BH_4)_2$ (black line) desorbed at 300 °C (a) and TPD data for those products further desorbed at 600 °C (b).

the sample with additives was adjusted by the actual percentage of $Mg(BH_4)_2$ present to account for the fact that only the borohydride species, and not the additives, is releasing the hydrogen. In this way, the weight percent of hydrogen released for the sample ± additives can accurately be compared. Residual gas analysis (RGA) of both the $Mg(BH_4)_2$ ± additives confirmed that the primary gaseous species was hydrogen, with a small percentage identified as various volatile B_xH_y species (Figure 3). The sample with additives also released hydrogen much faster: 95% of hydrogen desorption was completed within the first two hours compared to the ten hours needed for the sample without additives.

Prior to TPD studies, $Mg(BH_4)_2$ ± additives were ball-milled to reduce the grain size of the borohydride particles and, when additives were introduced, to thoroughly incorporate them homogenously throughout the borohydride material. In addition to the extreme broadening of the α-$Mg(BH_4)_2$ reflections, there is pXRD evidence that partial conversion from α to β-phase occurred during the milling process. Instead of distinct β-phase peaks, the presence of additives contributed to broadness at 18.8°, where the strongest reflection from β-$Mg(BH_4)_2$ would normally be observed (see the Supporting Information, Figure S1-a and b).

Solid state ^{11}B MAS NMR spectra (Figure S1-c and d) obtained for both samples, as well as the premilled $Mg(BH_4)_2$, confirms the partial α to β phase change after ball milling from the eminent peak shift of −39.6 ppm to −40.7 ppm. The feature at −40.7 ppm was previously reported to be the major peak of β-phase-$Mg(BH_4)_2$.[30] Ball-milling with additives also revealed the same peak, as well as peaks in the −10 and −30 ppm range,

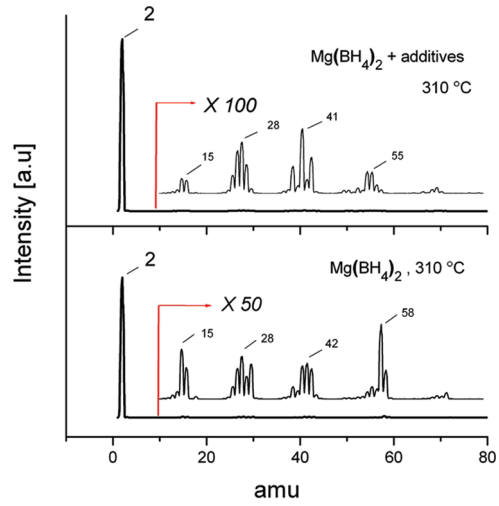

Figure 3. Residual gas analysis (RGA) of $Mg(BH_4)_2$ with and without TiF_3 and $ScCl_3$ additives at 310 °C. Peaks labeled at 2 amu are from hydrogen, which is the primary species evolving for both samples. The amu range from 10−80 is magnified and general peak positions are labeled to illustrate the small quantity of other gaseous species released at this temperature.

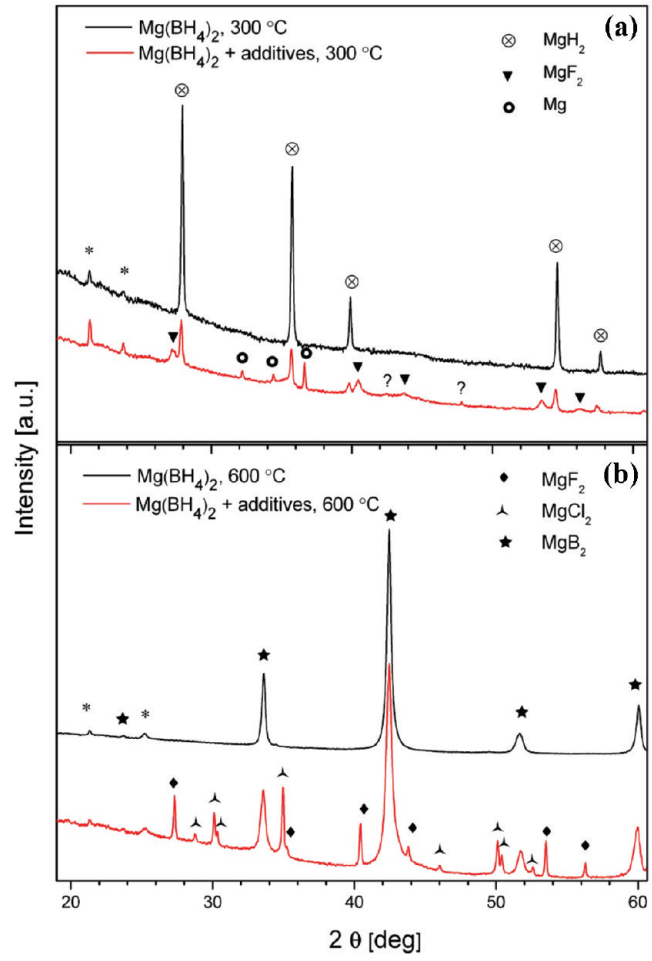

Figure 4. pXRD patterns for $Mg(BH_4)_2$ with (red line) and without 5 mol % TiF_3 and $ScCl_3$ (black line) after TPD characterization at 300 °C (a). Pure $Mg(BH_4)_2$ shows only MgH_2, but with the addition of TiF_3 and $ScCl_3$, Mg and MgF_2 are observed as well. An asterisk (*) denotes peaks from the sample holder and the question marks (?) represent unidentified peaks. At 600 °C (b), the pattern shows only MgB_2 for $Mg(BH_4)_2$ without additives. With additives, MgF_2 and $MgCl_2$ are also present.

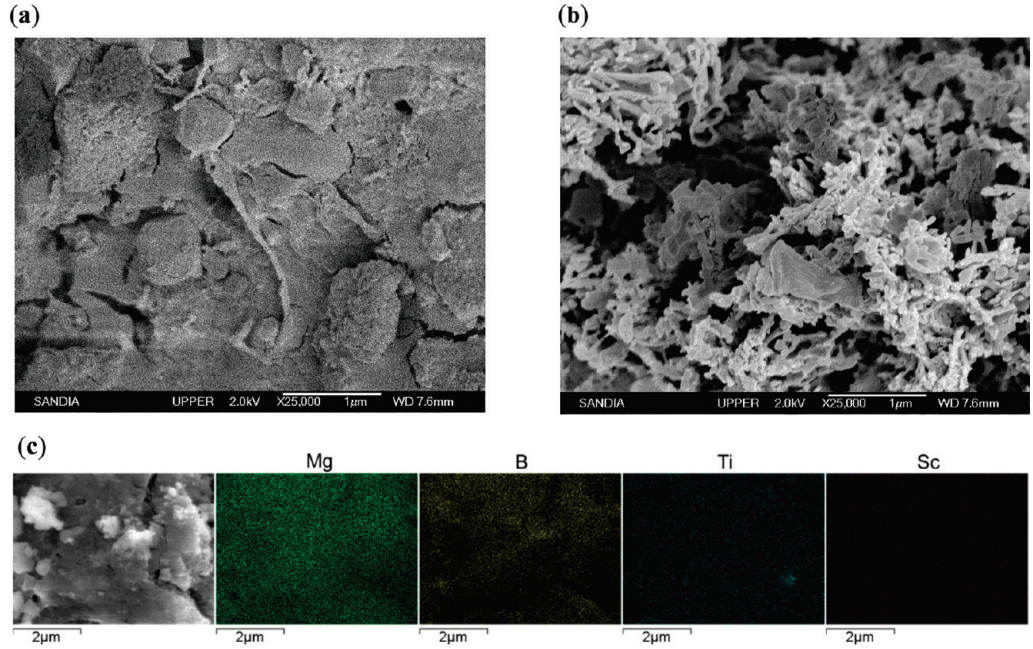

Figure 5. SEM images of MgB_2 formed from the complete hydrogen release of $Mg(BH_4)_2$ with (a) and without (b) additives present. Elemental mapping of $Mg(BH_4)_2$ with additives after complete hydrogen release shows homogeneous distribution of Ti and Sc atoms (c).

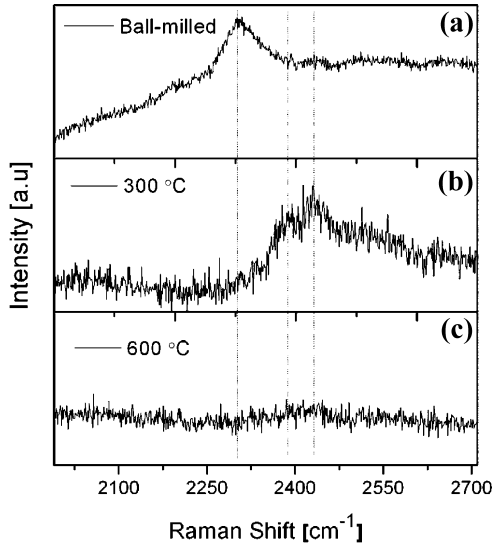

Figure 6. Raman spectra for $Mg(BH_4)_2$ with 5 mol % TiF_3, $ScCl_3$ after ball-milling (a), after the first desorption at 300 °C (b), and after the second desorption at 600 °C (c). Vertical lines emphasize the shift in peak position(s) from 2300 cm^{-1} for the ball-milled sample (a) to peaks at 2386 and 2432 cm^{-1} for the sample with additives (b). A broad feature extending from 2473 to 2583 cm^{-1} is also observed. After heating at 600 °C (c), the features present in (a) and (b) are not seen.

which suggest that a preliminary chemical reaction occurred. Boron oxide contaminants, indicated by broad peaks between −5 and 20 ppm (BO_3 and B−OH type), accounted for less than 5% of the total boron present and most likely formed during sample handling and transportation between institutions.

Powder XRD showed that TiF_3 reflections remained strong throughout the milling process, however no peaks belonging to $ScCl_3$ were identified due to its semiamorphous nature. In contrast, ^{45}Sc MAS NMR clearly indicated that more than 40% of $ScCl_3$ (peak at 222.9 ppm) was present in the material. The rest (∼60%) of Sc signal appeared as a broad peak at 133.2 ppm and may correspond to mixed $ScCl_x(BH_4)_y$ species or scandium oxide contaminants.[47,48] Formation of ScF_3 or a species with F coordination to Sc was excluded due to distinctive difference in their chemical shifts,[49] i.e. −52 ppm for ScF_3. ^{45}Sc MAS NMR confirmed that no ScB_2 (resonance at ∼760 ppm) or ScH_2 (>600 ppm) were present. Further spectroscopic characterization is under investigation to uniquely identify the new scandium species.

Titanium is well-known as an effective dopant for reducing the temperature for hydrogen release in metal hydrides and other systems.[5,38,43] However, the mechanism of action is still not completely understood. Recent work on low-temperature hydrogen release in $LiBH_4$ with a stoichiometric addition of TiF_3 gave evidence for the formation of $Ti(BH_4)_3$ *in situ* at temperatures above 70 °C.[41] Because $Ti(BH_4)_3$ is unstable at room temperature, it was proposed that elevated temperatures resulted in immediate hydrogen evolution following $Ti(BH_4)_3$ formation.[17,34,41]

The role of scandium during desorption is not clear, although experiments run without the addition of 5 mol % $ScCl_3$ showed less kinetic enhancement in addition to slightly reduced hydrogen evolution at 300 °C (data not shown).

Powder XRD patterns of both samples after desorption at 300 °C (Figure 4a) show MgH_2 formation. This is a well-known product of $Mg(BH_4)_2$ decomposition at that temperature.[28–30,50] Soloveichick et al. proposed that the decomposition of $Mg(BH_4)_2$ to MgH_2 is the first step (1) of the multistep process[30]

$$6Mg(BH_4)_2 \rightarrow 5MgH_2 + MgB_{12}H_{12} + 13H_2 \quad (1)$$

$$5MgH_2 \rightarrow 5Mg + 5H_2 \quad (2)$$

$$5Mg + MgB_{12}H_{12} \rightarrow 6MgB_2 + 6H_2 \quad (3)$$

With additives, there is pXRD evidence of Mg and MgF_2 in addition to MgH_2 (Figure 4a). The presence of MgH_2 and Mg indicates that both reactions 1 and 2 are occurring to some extent. MgF_2 implies partial reaction of TiF_3 with $Mg(BH_4)_2$, possibly forming Ti-containing borohydride species which can then readily decompose to release hydrogen. However, if this

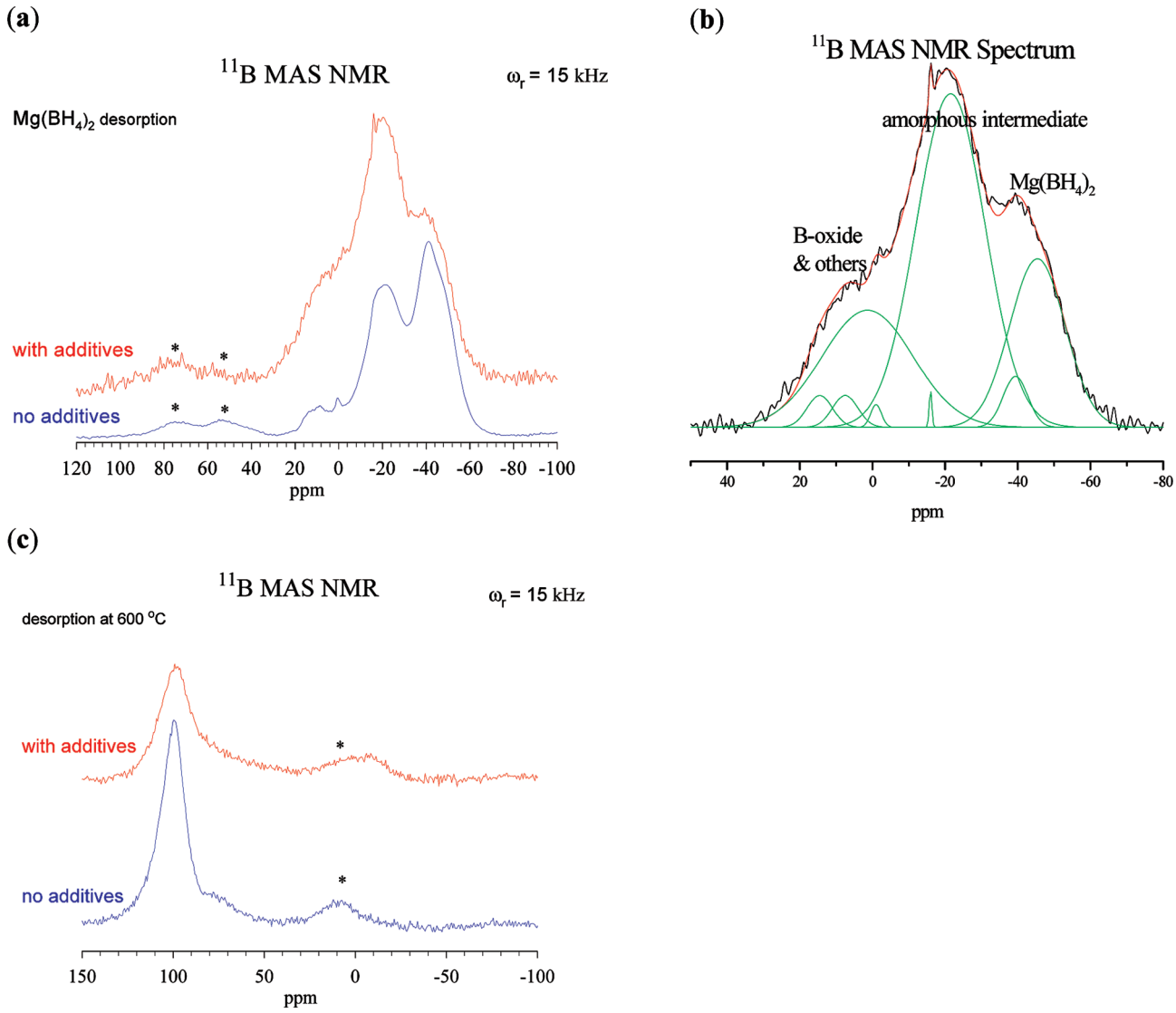

Figure 7. ^{11}B MAS NMR spectra for $Mg(BH_4)_2$ with (red line) and without additives (black line) (a) after the first desorption reaction at 300 °C; (b) deconvolution of ^{11}B MAS NMR spectrum for $Mg(BH_4)_2$ with additives after desorption at 300 °C; (c) after the second desorption at 600 °C.

was the case, TiB_2 species, which were not observed in our study, would be anticipated as products in the desorbed samples. The titanium cation is known to catalyze hydrogen release in MgH_2[51,52] and borohydrides.[5,41,43] However, recent work using XPS has shown that the fluoride anion may also play a role in enhancing the desorption and rehydrogenation by forming catalytically active Ti−F−Mg species in addition to inactive MgF_2.[53] The additional hydrogen released at 300 °C for the sample with additives may be due to destabilization of MgH_2 by the titanium cation as well as the fluoride anion, which would explain the observation of Mg as a product of reaction 2, at this temperature. No crystalline peaks could be attributed to the predicted *C*2/*m* structure of $MgB_{12}H_{12}$.[54]

A second desorption was performed at 600 °C to release the remaining hydrogen and produce the fully desorbed state, MgB_2. The sample with additives released 3.3 wt % of hydrogen, while the sample without catalysts released an additional 6.3 wt % of hydrogen (Figure 2b). Adding these values to the percent weight loss from the first desorption at 300 °C gives a total weight loss of 14% and 13% for the pristine sample and the sample with additives, respectively. Since $Mg(BH_4)_2$ has a theoretical hydrogen weight percentage of 14.9%. This leaves a few percent of hydrogen unaccounted for in the samples. In addition to the hydrogen which is lost as volatile B_xH_y species, it is possible that some hydrogen was released during the high-energy ball-milling process, which can generate high local temperatures. The new ^{11}B MAS NMR peaks which appeared near −10−30 ppm after ball-milling may explain such hydrogen release. Also, a small amount of hydrogen might remain in the sample at 600 °C in the form of stable $[B_{12}H_{12}]^{2-}$-type intermediates. Powder XRD confirmed the formation of MgB_2 as the final decomposition product. In the sample with additives, MgF_2 and $MgCl_2$ were detected as anticipated, while no crystalline peaks associated with Ti and Sc were identified (Figure 4b).

SEM images after the second desorption at 600 °C revealed distinct morphologies of the two samples (Figure 5). The MgB_2 (Figure 5b) was composed of many submicrometer branches whereas the MgB_2 with additives appeared to be composed of both spherical particles and planar structures, with comparatively less surface area (Figure 5a). Elemental mapping of the MgB_2 with additives showed a homogeneous distribution of Ti and Sc atoms throughout the sample (Figure 5c).

Raman spectroscopy was used to characterize $Mg(BH_4)_2$ before and after ball-milling following the first and second

TABLE 1: Proposed Boron Species from the Deconvolution Analysis of ^{11}B MAS NMR Spectra of $Mg(BH_4)_2$ with Additives and without after Desorption at 300 °C

	chemical shift (ppm)	relative quantity	
		no additives	with additives
B_2O_3 or B−OH type oxide contaminant	20−0	0.03	0.04
amorphous	2.2	0.06	0.23
$MgB_{12}H_{12}$	−16.8	0.01	<0.002
early stage intermediates	−21.8	0.43	0.5
$Mg(BH_4)_2$-I	−39.4	0.06	0.03
$Mg(BH_4)_2$-II	−45.4	0.41	0.2

desorption at 300 and 600 °C, respectively (Figure 6). The strong peaks of the $Mg(BH_4)_2$ (Figure S2) agree well with literature.[24] The B−H stretching mode of the $[BH_4]^-$ anion is centered at 2300 cm^{-1} with weaker bending modes observed at 2200, 1394, and 1200 cm^{-1}. After ball-milling, both $Mg(BH_4)_2$ samples showed significant broadening of the peak at 2300 cm^{-1}. Ball milling generally results in the broadening of Raman peaks, as it can increase the density of defects and widen bond length distribution. Raman measurement of pure $Mg(BH_4)_2$ after the first and second desorptions did not reveal any observable peaks. However, the Raman spectrum of $Mg(BH_4)_2$ with additives showed a disappearance of the 2300 cm^{-1} peak and appearance of several new peaks at 2387, 2442, and 2509 cm^{-1} after the first desorption (Figure 6). Hydrated $MgB_{12}H_{12}$ synthesized in our lab showed prominent Raman features at 2474 and 2515 cm^{-1} (Figure S2), which agree well with the Raman spectrum anticipated for the $[B_{12}H_{12}]^{2-}$ anion.[55] The new peaks observed for $Mg(BH_4)_2$ with additives after the first desorption may be due to $Mg(B_xH_y)_n$ species, such as $MgB_{12}H_{12}$, which is a proposed decomposition product of $Mg(BH_4)_2$ at temperatures around 300 °C.[30,26,31]

According to ^1H MAS NMR spectra for the two systems, dehydrogenation proceeded much further for the $Mg(BH_4)_2$ at 300 °C with additives, as integration of its hydrogen peak was only 30% of that for pure $Mg(BH_4)_2$ (Figure S3-a), further confirming the additive effect seen in the TPD data at 300 °C

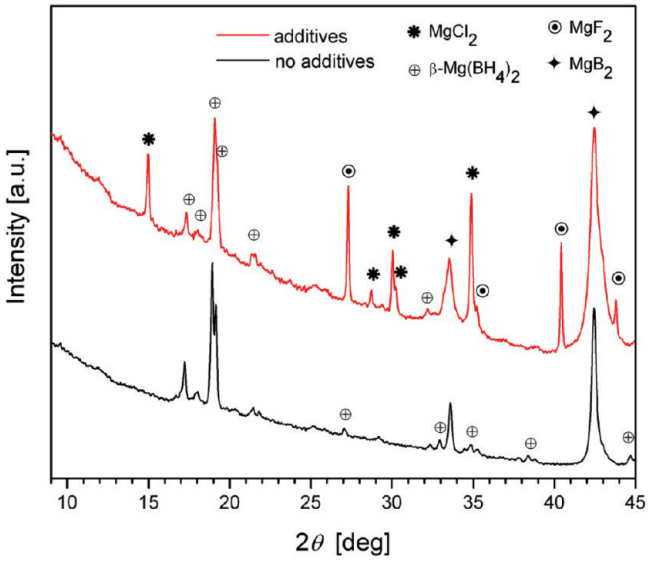

Figure 8. pXRD of the sample with additives and without additives after rehydrogenation at 900 bar H_2, 390 °C for 72 h. β-$Mg(BH_4)_2$ and MgB_2 are identified for both samples. The sample with TiF_3 and $ScCl_3$ originally added also shows $MgCl_2$ and MgF_2 formation.

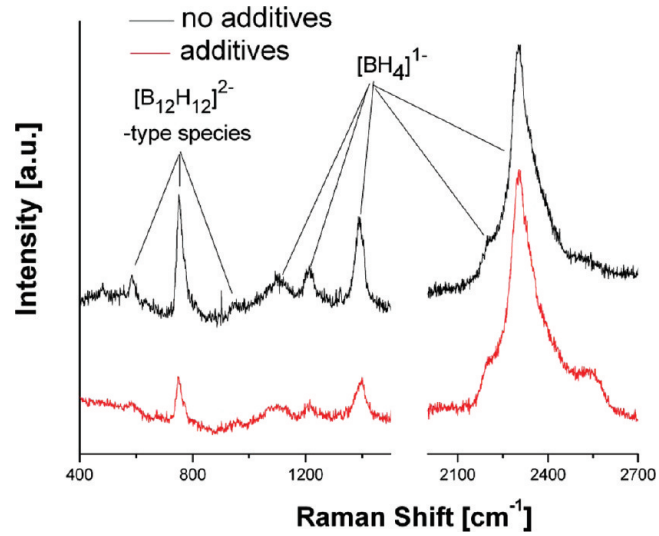

Figure 9. Raman spectra of products after rehydrogenation experiments. The black and red spectra are from the samples with TiF_3 and $ScCl_3$ additives and without, respectively, after the rehydrogenation experiment. The strong peak at 2300 cm^{-1} and weaker modes at 1391, 1211, and 1106 cm^{-1} are from $Mg(BH_4)_2$ and the peaks observed at 752 and 584 cm^{-1} could be from $MgB_{12}H_{12}$ or a species similar in structure.

(Figure 2a). The formation of MgF_2 was also confirmed by ^{19}F MAS NMR (Figure S3-d, peak at −198.7 ppm) after decomposition. No other fluorine species was detected. Decomposition of $Mg(BH_4)_2$ produced mostly unidentifiable amorphous intermediates, indicated by ^{11}B MAS NMR peaks from 0 to −30 ppm (Figure 7). When the ^{11}B MAS NMR spectra were compared, the extent of reaction progress with additives is evidenced by lower concentration of the residual $Mg(BH_4)_2$ (peaks ∼ −40 ppm) and increased intensity of broad peaks at ∼ −22 and ∼2 ppm (Figure 7a). The deconvolution of the ^{11}B MAS NMR spectra for the sample with additives is shown in Figure 7b and a summary of the proposed species from the curve fitting is listed in Table 1 for both samples. The peak at 2 ppm may be attributed to amorphous boron as supported by ^{11}B CPMAS NMR data (Figure S3) that showed no CP signal of the peak. Boron species with direct B−H bonds should appear in the CPMAS NMR experiment since dipolar coupled B−H spin pairs are readily probed by this method. The reaction intermediate peak at ∼−22 ppm has been previously observed[30] when the decomposition temperature is low and is believed to contain $Mg(B_xH_y)_n$ moieties. This moiety may be a precursor to $[B_{12}H_{12}]^{2-}$ species formation and is labeled as an "early stage intermediate" in Table 1. Interestingly, half of the boron content for both samples is partitioned in the form of this "early stage intermediate". These data are consistent with Raman results that also suggest the formation of $Mg(B_xH_y)_n$ moieties after desorption at 300 °C (Figure 6). The ^{11}B MAS NMR measurement (Figure 7c) conducted after the second desorption at 600 °C indicated almost complete dehydrogenation for samples ± additives. Furthermore, this measurement showed that MgB_2 (∼97 ppm) was the primary boron-containing species formed, though a $[B_{12}H_{12}]^{2-}$-type intermediate was present in negligibly small quantity as evidenced by ^{11}B CPMAS spectra (Figure S3-c). Use of additives appears to have lowered the conversion efficiency from the intermediate to MgB_2. NMR also confirmed that the formation of TiB_2 did not occur within the detection limit. ScB_2 formation is not obvious, but its presence cannot be unambiguously determined by ^{11}B NMR (∼90 ppm) due to possible overlap with MgB_2. Overall, the formation of amor-

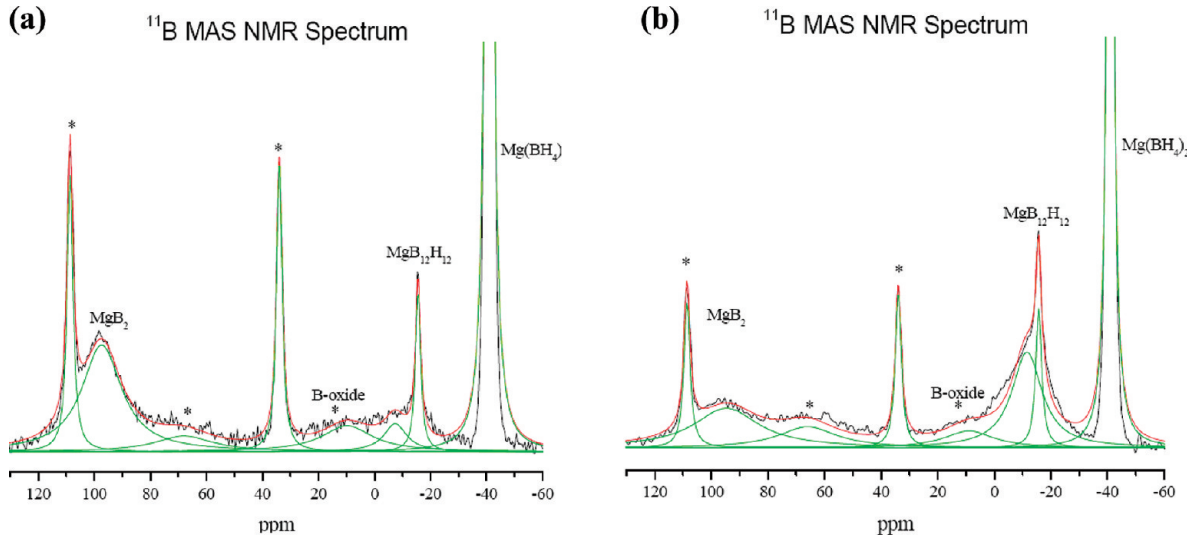

Figure 10. Deconvolution of ^{11}B MAS NMR of samples after the rehydrogenation reaction with (b) and without additives (a). Both show $Mg(BH_4)_2$ (∼−42 ppm), MgB_2 (∼97 ppm) and boron-containing intermediate species (∼−11 ppm, −15 ppm). Percentages of species present based on the deconvolution analysis are presented in Table 2. Asterisks (*) indicate spinning side bands.

phous $Mg(B_xH_y)_n$ at low temperatures indicates the complex nature of the decomposition pathway. The end product of decomposition at 600 °C, however, is the single phase, simple compound, MgB_2, with a negligible quantity of a $B_{12}H_{12}$-related species.

Once the products of dehydrogenation had been characterized, these materials were then subjected to 90 MPa H_2 at 390 °C for 72 h and similarly characterized with pXRD, Raman, and NMR spectroscopy. Visually, the sample with additives showed formation of a white powder on top of the original brown pellet (Figure S4-b). The rehydrogenation of the decomposition products from the $Mg(BH_4)_2$ without additives generated significantly less white material (Figure S4-d). Identification of the white powder proved challenging due to the difficulty in handling the powder and the lack of crystallinity. For that reason, in order to obtain an accurate representation of all species formed and their relative quantities, we ground the entire sample after rehydrogenation for further characterization.

Powder XRD of the samples following high-pressure treatment showed β-$Mg(BH_4)_2$ formation as well as unreacted MgB_2 in the samples with and without additives (Figure 8). The sample without additives showed a doublet with peaks at 18.9° and 19.2°. For the sample with additives, there was a peak centered at 19.1° and a shoulder at 19.2°. This broadening of this peak may indicate that β-$Mg(BH_4)_2$ is less crystalline in the sample with additives. Raman spectroscopy also confirmed the rehydrogenation of MgB_2 to $Mg(BH_4)_2$. The strong peak at 2300 cm^{-1} is characteristic of the B−H stretch in the $[BH_4]^{-1}$ anion (Figure 9) and was originally observed for the synthesized product (Figure S2). In addition, the weaker modes associated with B−H bending were present at 1391, 1211, and 1106 cm^{-1}. Additional peaks observed at 752 and 584 cm^{-1} align with experimentally observed peaks for hydrated $MgB_{12}H_{12}$ (Figure S2) and literature values for the $[B_{12}H_{12}]^{-2}$ anion.[55] According to Muetterties et al., the peaks at 752 and 584 cm^{-1} are due to the in-phase breathing mode of the boron shell.[55] A broad peak at 2530 cm^{-1} was also observed that is near the literature value of 2518 cm^{-1} assigned to the out-of-phase breathing mode of the hydrogen shell of the $[B_{12}H_{12}]^{-2}$ anion.[55] These results suggest that in addition to $Mg(BH_4)_2$, other $Mg(B_xH_y)_n$ moieties such as $MgB_{12}H_{12}$ formed in non-negligible amounts.

^{11}B MAS NMR also confirmed rehydrogenation of MgB_2 to $Mg(BH_4)_2$ after the high-pressure experiment, as evidenced by the sharp peak at ∼−41 ppm (Figure 10). A closer examination of the ^{11}B MAS NMR spectra showed a broad signal (∼−11 ppm) near the $MgB_{12}H_{12}$ peak (∼−15.5 ppm), which is believed to be the same species in an amorphous state (Figure 10). This broad feature is much more visible in the sample with additives and accounts for ∼23% of the sample, in contrast to ∼4% for the sample without additives. The remaining MgB_2 was measured at 21% and 25% of the total sample with and without additives, respectively (Table 2). NMR estimated that the conversion to $Mg(BH_4)_2$ was ∼49% and ∼66% complete for samples ± additives, respectively. In general, the significant $Mg(BH_4)_2$ formation from MgB_2 produced at 600 °C confirms the reversibility of this system, as first discovered by Severa et al.[44] While the additives used in this study significantly improved the desorption of $Mg(BH_4)_2$ at 300 °C, they increased the undesirable amorphous boron−hydrogen species, $Mg(B_xH_y)_n$ formed during the rehydrogenation reaction from ∼4% for the MgB_2 without additives, to ∼23% (Table 2).

TABLE 2: Proposed Boron Species Based on Deconvolutions of ^{11}B MAS NMR Spectra of Samples after the Rehydrogenation Reaction (Figure 9)

		relative quantity	
	chemical shift (ppm)	no additives	with additives
MgB_2	97.3	0.25	0.21
amorphous[a]	−11	0.04	0.23
$MgB_{12}H_{12}$	−15.5	0.05	0.07
$Mg(BH_4)_2$	−40.95	0.66	0.49

[a] Amorphous phase in this system indicates $[B_{12}H_{12}]^{2-}$ related species.

We are currently investigating the effect of other metal halides on the hydrogen storage properties of $Mg(BH_4)_2$. Both improving the MgB_2 hydrogenation efficiency and limiting the amount of stable intermediate species formed are critical for the additive search. In this study we show that additives can alter both the hydrogen release and absorption reactions. The mechanisms by which additives affect (stabilize or destabilize) the intermediates during the dehydrogenation and subsequent rehydrogenation of $Mg(BH_4)_2$ represent interesting and fundamental questions that require further studies. A better understanding of their involvement could lead to the correct combinations of various additives which ideally would enhance incorporation of hydrogen into

the MgB_2 lattice during the rehydrogenation reaction in addition to improving hydrogen desorption.

Conclusions

We have shown that addition of 5 mol % of TiF_3 and $ScCl_3$ to $Mg(BH_4)_2$ significantly improves the hydrogen desorption kinetics. With additives, hydrogen desorption reaches 95% completion five times faster than without additives. Moreover, when additives are present more hydrogen is released at 300 °C because the additives destabilize MgH_2 in addition to $Mg(BH_4)_2$. Raman and NMR spectroscopy confirm the presence of amorphous $Mg(B_xH_y)_n$ intermediates, possibly including $[B_{12}H_{12}]^{2-}$ and related species. NMR and Raman measurements from the desorbed samples at 300 °C showed that there is very likely an "early stage intermediate" similar to but distinct from $MgB_{12}H_{12}$ that acts as a precursor for its eventual formation at higher temperatures. During the decomposition at 300 °C, the additives seem to promote the formation of the early stage intermediates, which may be responsible for the enhanced kinetics. At 600 °C, the material decomposes primarily to MgB_2.

We confirmed with pXRD, Raman and NMR spectroscopy that during hydrogenation there is significant conversion of MgB_2 to the fully hydrogenated $Mg(BH_4)_2$ with and without additives. However, the presence of additives seems to promote the formation of stable boron−hydrogen intermediates during rehydrogenation.

Acknowledgment. The authors would like to thank George Sartor, Ken Stewart, and Jeff Chames for their skillful technical assistance. Assistance in sample handling by Joseph Reiter at JPL and David Abrecht at Caltech are greatly appreciated. We would also like to thank Craig Jensen, Ewa Rönnebro, Joe Cordaro, and Mitch Anstey for helpful discussions. We gratefully acknowledge financial support from the U.S. Department of Energy, Office of Energy Efficiency and Renewable Energy, in the Hydrogen, Fuel Cells & Infrastructure Technologies Program under Contract Nos. DE-AC04-94AL85000, DE-AI-01-05EE11104, and DE-AI-01-05EE11105. The NMR facility at Caltech was supported by the National Science Foundation (NSF) under Grant Number 9724240 and partially supported by the MRSEC Program of the NSF under Award Number DMR-0520565. JZZ is grateful to support by the Basic Energy Sciences (BES) Division of the US Department of Energy (DOE) (DE-FG02-06ER46251).

Supporting Information Available: Additional NMR results, pXRD patterns after ball-milling, Raman spectra and images of samples after rehydrogenation. This material is available free of charge via the Internet at http://pubs.acs.org.

References and Notes

(1) Jones, R. H.; Thomas, G. J. *Materials for the hydrogen economy*; CRC Press: Boca Raton, FL, 2007.
(2) Satyapal, S.; Petrovic, J.; Read, C.; Thomas, G.; Ordaz, G. *Catal. Today* **2007**, *120*, 246.
(3) Schlapbach, L.; Züttel, A. *Nature* **2001**, *414*, 353.
(4) Walker, G. S. *Solid State Hydrogen Storage*; Woodhead Publishing Limited: Cambridge, U.K., 2008.
(5) Bogdanović, B.; Schwickardi, M. *J. Alloys Comp.* **1997**, *253−254*, 1.
(6) Yu, X. B.; Grant, D. M.; Walker, G. S. *J. Phys. Chem. C* **2009**, *113*, 17945.
(7) Pendolino, F.; Mauron, P.; Borgschulte, A.; Züttel, A. *J. Phys. Chem. C* **2009**, *113*, 17231.
(8) Yang, J.; Hirano, S. *Adv. Mater.* **2009**, *21*, 3023.
(9) Lee, J. Y.; Ravnsbaek, D.; Lee, Y. S.; Kim, Y.; Cerenius, Y.; Shim, J. H.; Jensen, T. R.; Hur, N. H.; Cho, Y. W. *J. Phys. Chem. C* **2009**, *113*, 15080.
(10) Dorthe, R.; Yaroslav, F.; Yngve, C.; Hans, J. J.; Flemming, B.; Jørgen, S.; Torben, R. J. *Angew. Chem., Int. Ed.* **2009**, *48*, 6659.
(11) Mao, J. F.; Yu, X. B.; Guo, Z. P.; Liu, H. K.; Wu, Z.; Ni, J. *J. Alloys Comp.* **2009**, *479*, 619.
(12) Mao, J. F.; Yu, X. B.; Guo, Z. P.; Poh, C. K.; Liu, H. K.; Wu, Z.; Ni, J. *J. Phys. Chem. C* **2009**, *113*, 10813.
(13) Kim, C.; Hwang, S. J.; Bowman, R. C.; Reiter, J. W.; Zan, J. A.; Kulleck, J. G.; Kabbour, H.; Majzoub, E. H.; Ozolins, V. *J. Phys. Chem. C* **2009**, *113*, 9956.
(14) Ibikunle, A.; Goudy, A. J.; Yang, H. *J. Alloys Comp.* **2009**, *475*, 110.
(15) Pinkerton, F. E.; Meyer, M. S.; Meisner, G. P.; Balogh, M. P.; Vajo, J. J. *J. Phys. Chem. C* **2007**, *111*, 12881.
(16) Vajo, J. J.; Skeith, S. L.; Mertens, F. *J. Phys. Chem. B* **2005**, *109*, 3719.
(17) Hoekstra, H. R.; Katz, J. J. *J. Am. Chem. Soc.* **1949**, *71*, 2488.
(18) Konoplev, V. N.; Bakulina, V. M. *Russ. Chem. Bull.* **1971**, *20*, 136.
(19) Plesek, J.; Hermanek, S. *Collect. Czech. Chem. Commun.* **1966**, *31*, 3845.
(20) Stasinevich, D. S.; Egorenko, G. A. *Russ. J. Inorg. Chem.* **1968**, *13*, 341.
(21) Wiberg, E.; Bauer, R. *Naturforsch. A* **1950**, *5*, 689.
(22) Chłopek, K.; Frommen, C.; Leon, A.; Zabara, O.; Fichtner, M. *J. Mater. Chem.* **2007**, *17*, 3496.
(23) Her, J.-H.; Stephens, P. W.; Gao, Y.; Soloveichik, G. L.; Rijssenbeek, J.; Andrus, M.; Zhao, J.-C. *Acta Cryst. B* **2007**, *63*, 561.
(24) Cerný, R.; Filinchuk, Y.; Hagemann, H.; Yvon, K. *Angew. Chem., Int. Ed.* **2007**, *46*, 5765.
(25) Kuznetsov, V. A.; Dymova, T. N. *Russ. Chem. Bull.* **1971**, *20*, 204.
(26) Matsunaga, T.; Buchter, F.; Mauron, P.; Bielman, M.; Nakamori, Y.; Orimo, S.; Ohba, N.; Miwa, K.; Towata, S.; Züttel, A. *J. Alloys Comp.* **2008**, *459*, 583.
(27) Sarner, S. F. *Propellant chemistry*; Van Nostrand Reinhold Inc.: New York, 1966.
(28) Li, H. W.; Kikuchi, K.; Nakamori, Y.; Ohba, N.; Miwa, K.; Towata, S.; Orimo, S. *Acta Mater.* **2008**, *56*, 1342.
(29) Hanada, N.; Chłopek, K.; Frommen, C.; Lohstroh, W.; Fichtner, M. *J. Mater. Chem.* **2008**, *18*, 2611.
(30) Soloveichik, G. L.; Gao, Y.; Rijssenbeek, J.; Andrus, M.; Kniajanski, S.; Bowman, R. C.; Hwang, S. J.; Zhao, J. C. *Int. J. Hydrogen Energy* **2009**, *34*, 916.
(31) Li, H. W.; Miwa, K.; Ohba, N.; Fujita, T.; Sato, T.; Yan, Y.; Towata, S.; Chen, M. W.; Orimo, S. *Nanotechnology* **2009**, *20*, 204013.
(32) Nakamori, Y.; Miwa, K.; Ninomiya, A.; Li, H.; Ohba, N.; Towata, S.; Züttel, A.; Orimo, S. *Phys. Rev. B* **2006**, *74*, 45126.
(33) Nakamori, Y.; Li, H. W.; Miwa, K.; Towata, S.; Orimo, S. *Mater. Trans.* **2006**, *47*, 1898.
(34) Marks, T. J.; Kolb, J. R. *Chem. Rev.* **1977**, *77*, 263.
(35) Bhakta, R. K.; Herberg, J. L.; Jacobs, B.; Highley, A.; Behrens, R.; Ockwig, N. W.; Greathouse, J. A.; Allendorf, M. D. *J. Am. Chem. Soc.* **2009**, *131*, 13198.
(36) Rönnebro, E.; Majzoub, E. H. *J. Phys. Chem. B* **2007**, *111*, 12045.
(37) Kim, J. H.; Shim, J. H.; Cho, Y. W. *J. Power Sources* **2008**, *181*, 140.
(38) Bogdanović, B.; Felderhoff, M.; Kaskel, S.; Pommerin, A.; Schlichte, K.; Schüth, F. *Adv. Mater.* **2003**, *15*, 1012.
(39) Bogdanović, B.; Felderhoff, M.; Germann, M.; Härtel, M.; Pommerin, A.; Schüth, F.; Weidenthaler, C.; Zibrowius, B. *J. Alloys Comp.* **2003**, *350*, 246.
(40) Hagemann, H.; Longhini, M.; Kaminski, J. W.; Wesolowski, T. A.; Cerný, R.; Penin, N.; Sørby, M. H.; Hauback, B. C.; Severa, G.; Jensen, C. M. *J. Phys. Chem. A* **2008**, *112*, 7551.
(41) Fang, Z. Z.; Ma, L. P.; Kang, X. D.; Wang, P. J.; Wang, P.; Cheng, H. M. *Appl. Phys. Lett.* **2009**, *94*, 044104.
(42) Fichtner, M.; Zhao-Karger, Z.; Hu, J.; Roth, A.; Weidler, P. *Nanotechnology* **2009**, *20*, 204029.
(43) Li, H. W.; Kikuchi, K.; Nakamori, Y.; Miwa, K.; Towata, S.; Orimo, S. *Scr. Mater.* **2007**, *57*, 679.
(44) Severa, G.; Rönnebro, E.; Jensen, C. M. *Chem. Commun.* **2010**, *46*, 421.
(45) Zanella, P.; Crociani, L.; Masciocchi, N.; Giunchi, G. *Inorg. Chem.* **2007**, *46*, 9039.
(46) Hwang, S. J.; Bowman, R. C.; Reiter, J. W.; Rijssenbeek, J.; Soloveichik, G. L.; Zhao, J. C.; Kabbour, H.; Ahn, C. C. *J. Phys. Chem. C* **2008**, *112*, 3164.
(47) Kim, N.; Hsieh, C. H.; Stebbins, J. F. *Chem. Mater.* **2006**, *18*, 3855.
(48) Riou, D.; Fayon, F.; Massiot, D. *Chem. Mater.* **2002**, *14*, 2416.
(49) Lo, A. Y. H.; Sudarsan, V.; Sivakumar, S.; van Veggel, F.; Schurko, R. W. *J. Am. Chem. Soc.* **2007**, *129*, 4687.
(50) Matsunaga, T.; Buchter, F.; Mauron, P.; Bielman, A.; Nakamori, Y.; Orimo, S.; Ohba, N.; Miwa, K.; Towata, S.; Züttel, A. *J. Alloys Comp.* **2008**, *459*, 583.

(51) Choi, Y. J.; Lu, J.; Sohn, H. Y.; Fang, Z. Z.; Rönnebro, E. *J. Phys. Chem. C* **2009**, *113*, 19344.
(52) Du, A. J.; Smith, S. C.; Yao, X. D.; Lu, G. Q. *J. Phys. Chem. B* **2006**, *110*, 21747.
(53) Ma, L. P.; Kang, X. D.; Dai, H. B.; Liang, Y.; Fang, Z. Z.; Wang, P. J.; Wang, P.; Cheng, H. M. *Acta Mater.* **2009**, *57*, 2250.
(54) Ozolins, V.; Majzoub, E. H.; Wolverton, C. *J. Am. Chem. Soc.* **2009**, *131*, 230.
(55) Muetterties, E. L.; Merrifield, R. E.; Miller, H. C.; Knoth, W. H.; Downing, J. R. *J. Am. Chem. Soc.* **1962**, *84*, 2506.

JP9116744